Magnetization Controlling of Magnetic Probes in Spin-Polarized Scanning Tunneling Microscopy

Pin-Jui Hsu[1] and Minn-Tsong Lin[1,2,*]

[1] Department of Physics, National Taiwan University, 10617 Taipei, Taiwan
[2] Institute of Atomic and Molecule Sciences, Academia Sinica, 10617 Taipei, Taiwan
* e-mail: mtlin@phys.ntu.edu.tw

The state-of-the-art spin mapping technique of spin-polarized scanning tunneling microscopy (SP-STM) and spectroscopy (SP-STS) can provide information on magnetic domain and electronic structure with extremely high spatial resolution. This essentiality is desperate for the studying of interplay between structural, electronic and magnetic properties in various fascinating magnetic systems with low dimensionality. Based on spin dependent tunneling principle, the magnetization direction of spin-polarized probe plays an crucial role in identifying magnetic surface spin distribution and gives rise to a critical issue of controlling spin orientation of magnetic probes of SP-STM. In this chapter, both overview of previous studies and recent progress subject to magnetization controlling of magnetic probes in SP-STM will be highlighted.

Keywords spin-polarized scanning tunneling microscopy ; magnetic domain imaging; tip magnetization; magnetic anisotropy; magnetic nanostructure; ring-shaped probe; ; *In situ* switching of magnetization of magnetic probe

1. Introduction

It is well known that magnetic domain plays an important role in linking the microscopic spin structures with macroscopic magnetic properties to understand underlying magnetic behaviors of magnetic materials [1]. Besides, due to the increasing interests in either technological application or fundamental physics of magnetic nanostructures with low dimensionality, e.g., ultrathin films, nanowires, and nanoparticles etc., magnetic imaging techniques with high spatial resolution consequently are required. Start from the past few decades, many methods have been developed to extract the information related to the magnetic domain and in general, they can be categorized into two branches. Detecting magnetic dipolar field in order to map out the local distribution of magnetic flux emerged from sample is belong to the first one branch. As firstly introduced by Bitter in 1932 [2], the fine colloidal magnetite Fe2O3 particles are used to decorate on magnetic sample surface to sense the outspread stray fields and these particles will accumulate in the field gradient positions to form the so-called Bitter domain patterns. This method provides the sensitivity of weak magnetic fields with a few hundred A/m and reaches the resolution of around 100 nm due to the limitation of particle size can be prepared up to 10 nm [3]. Another approach is magnetic force microscopy (MFM) which attempts to record magnetic stray fields through mechanically scanning on the magnetic sample surface. The main working principle of MFM is to detect magnetostatic interaction between a magnetic tip and the stray field of sample [4]. The corresponding magnetostatic forces or forces gradients are measured and analyzed with respect to the lateral position of tip to obtain the domain images. The lateral resolution of this method achieves about 20 to 50 nm [5, 6] which has reached a considerable degree of industrial applications since the moderate spatial resolution is sufficient and can be also applied to air ambient conditions.

The second branch of magnetic imaging techniques is based on the employment of photons, electrons and neutrons interacting with spin-polarized electronic structures or local magnetic field within the atoms of magnetic materials. Take the magneto-optical Kerr effect (MOKE) for example, it's the most widely applied experimental method in the study of ultrathin ferromagnetic films. A beam of polarized light is incident into the magnetic sample, and the rotation of the polarization in the reflected light reveals the magnetic properties [7,8]. This method provides a reasonable surface sensitivity from a penetration depth of around 20 nm and can be also employed in the applied external magnetic field to obtain spatially averaged hysteresis curves of thin films. In addition, the MOKE microscopy can be applied to magnetic imaging, however, with ultimately limited spatial resolution about 300 nm by the wave length of the probing light [9]. For circumventing the limitation, MOKE has also been employed in the in scanning near-field optical microscopy (SNOM) and improve the later resolution up to 50 nm so far [10]. In Lorentz microscopy, a transmission electron microscope (TEM) is used to measure the deflection of an electron beam due to the magnetic induction as the electrons traverse the film, i.e., Lorentz effect. The signal is averaged over the film thickness, and stray fields above and below the sample also have signal contribution leading to a cancellation of the signal in certain geometries. Several modes in the application are used, e.g. the defocused or Fresnel mode, or the differential phase contrast mode, and the latter one can reach a resolution better than 10 nm [11]. Surface sensitive techniques have been also developed such as scanning electron microscopy with polarization analysis (SEMPA) and spin-polarized low energy electron microscopy (SPLEEM). In SEMPA, a finely focused unpolarized high energy electron beam (around 10 KeV) is scanned over the sample surface, and the spin polarization of the secondary electrons emitted from the sample is detected and analysed.

The lateral resolution limitation depends only on the beam width; the signal intensities, however, get extremely small eventually. This method allows us to measure all three magnetization components simultaneously. The first experiment was done by Koike *et al.* in 1987 [12]. The surface sensitivity is very high (around 1 nm probing depth), and the lateral resolution is about 20 nm up to date [13, 14]. There is a severe drawback of this technique that measurements in strong applied magnetic fields (up to 0.1 Tesla) are, except for very special cases, not possible. As for SPLEEM, it is a not scanning, but full field imaging method that allows much faster image acquisition time. The spin-polarized low energy electron beam (around 10 eV) is incident normal to the surface and only the specularly reflected beam is used for imaging. Due to the absence of multiple scattering, i.e., the spin-orbit interaction contributes no signal, so that the spin contrast in the reflected beam only arises from the exchange scattering of different inelastic paths between incident spin-polarized beam electrons parallel or antiparallel to spin-polarized electrons in the ferromagnetic materials. The lateral resolution is limited by the spherical and chromatic aberrations of the objective lens and presently is not better than 10 nm in practice. The vertical resolution is limited by the wavelength of the electrons and allows the imaging of monatomic steps and thickness variations via interference contrast [15]. Another technique is called photoelectron mission microscopy (PEEM), it detects the excited secondary electrons giving rise to the signal and providing a spatial resolution of around 20 nm. In addition, based on the principle of X-ray magnetic circular dichorism (XMCD), it is able to have element specificity which enables to detect the alignment of each element in alloys or in the multilayers [16]. Furthermore, in X-ray linear dichroism (XMLD) combined with PEEM, it is demonstrated recently to resolve magnetic domains of ultrathin layers of antiferromagnets (AFM) and ferromagnets (FM) systems. It opens a opportunity for a better understanding of the exchange bias effect in fundamental AFM/FM coupled systems [17].

Looking forward to higher spatial resolution is always one of the goals of magnetic domain imaging. Since the invention of STM in 1981 by Binning and Rohrer [18], this technique capable of resolving real space images of surface with atomic resolution has been successfully demonstrated. The schematic setup diagram of STM has been shown in the Fig.1. Basically, a small bias voltage between tip and sample leads to quantum mechanical tunneling current and piezoelectric actuators can be applied to precisely control the position by the feedback loop. Because the tunneling current is an exponential function of tip-sample distance, almost one order of magnitude of current variations per angstrom fulfills the high spatial resolution of STM. In addition, in early 1970s [19], the experimental technique of spin-polarized electron tunneling in FM-insulator-superconductor planar tunnel junctions has been well established. Therefore, as firstly proposed by Pierce [20] in 1988, with the spin-polarized tip applying to STM is possible to obtain the real space spin configuration imaging at the ultimate, atomic resolution of magnetic surface. Nowadays, spin-polarized STM (SP-STM) has been developed into a powerful and advanced tool for imaging surface spin structures down to atomic scale. Furthermore, there are three mainly different spin-polarized tips developed for realizing spin-polarized electron tunneling in the SP-STM technique, all of which will be introduced in the next section, including respective working principles, advantages and related important issues.

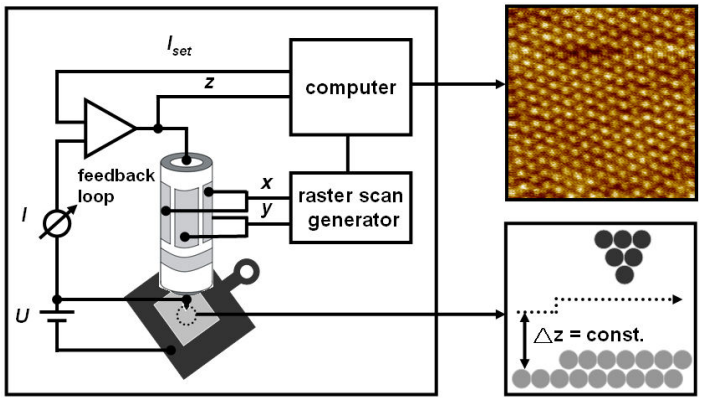

Fig. 1 Principle of STM in the topography (or constant current) mode. While the tip is laterally scans across the surface (controlled by the raster scan generator), the tunneling current is kept constant at a tunnel current position Iset. This is done by the feedback loop adjusting the z position of the tip. The respective tip displacement in z is then recorded as a function of the lateral position (x, y) (see inset in the bottom right). STM images are obtained by plotting z (x, y) in a color mode (see inset in the top right).

2. Spin-Polarized Scanning Tunneling Microscopy

2.1 Optically pumped GaAs tip

In this method, the GaAs tip optically pumped with circularly polarized light is used as the source of spin-polarized tunneling electrons [20]. By changing the helicity of the incident laser light, the sign of polarization of photon-excited electrons tunneling from GaAs can be easily reversed. This advantage is useful in separating magnetic from topographic and electronic effects in the spin-sensitive STM experiements. Besides, due to the photo-excited electrons polarized along the axis defined by the direction of incident laser light, the quantization axis of photo-excited electrons can be also modified by experimental geometry to detect either in-plane or out-of-plane spin configurations on the magentic

surface. Although the spin-polarized electron tunneling in STM with this method has been demonstrated by several groups [21-23], the unambiguous magnetic domain images still have not yet been observed. Some possible difficulties remain unresolved, for example, the polarization of incident light at the tip apex is not predicable and actually it may depend on the local tip position respect to the sample surface. Furthermore, it is also difficult to couple the incident light into non-symmetric tunneling vacuum gap without changing its polarization. These difficulties and even some more annoying problems [24-26] found recently cause this method not to be perfomed sucessfully in magnetic domain imaging.

2.2 Magnetic probe tip

As reported by Wiesendanger *et al.* [27] in 1990, the spin-polarized electron tunneling from ferromagnetic Cr_2O tip into Cr(001) single crystale surface has been observed by means of STM. The terraces separated by monatomic steps of around 0.14 nm height are obtained by using tungsten tip on the Cr(001) surface. After replcing the tungsten tip by a Cr_2O tip, due to the topological antiferromagnetism of Cr(001) surface as a result of self-consistent total-energy calculations [28], the apparent height periodically alternated from around 0.16 to 0.12 nm between the terraces are resolved. These additional contributions of around 14 % or peak to peak around 28 % to the tunneling current are refered to the spin-polarized electron tunneling. In addition, by applying the iron probe tips on Fe_3O_4 magnetite sample, the firt time that magnetic imaging down to the atomic level [29] has been realized by the SP-STM. Based on the principle of spin dependent tunneling [30] in Fig. 2 and lateral translation symmetry of magnetic spin structures [31], various spin structures with atomic resolution have been sucessfully demonstrated by the SP-STM technique operated at the constant current mode [32-36]. Besides using bulk materials as the magnetic probe tips, the magnetic thin film coated on tungsten tip is another way to prepare spin-polarized probes [37]. The polycrystalline tungsten tip is obtained by electrochemically etching and typically the diameter of a sharp tip end can be smaller than 100 nm. After transferring into the ultra-high vacuum (UHV) chamber, the *in situ* electron bombardment is treated to remove the oxide layers and contaminations of the tungsten tip. According to the magnetic materials coated on the tungsten tip, the spin sensitivity of different directions, e.g., in-plane or out-of-plane respect to the sample surface, can be selected by varying the thickness of magnetic thin films. Moreover, in order to reduce the influence of stray field emerged from spin-polarized tip on the magnetic sample, the coating of antiferromagnetic materials have also been used [38].

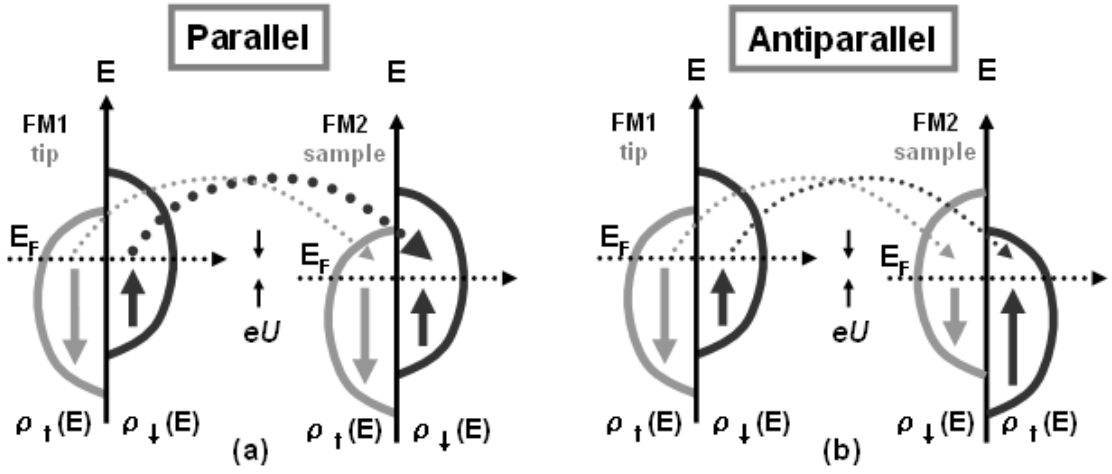

Fig. 2 Principle of spin dependent tunnelling between two ferromagnetic electrodes with a parallel orientation of the magnetization is depicted in (a) and an antiparallel orientation in (b). For elastic tunnelling and conservation of the spin, the tunnelling current is in case (a) larger than in case (b).

In addition to the constant current mode in STM for measuring the topological apparent height, the scanning tunneling spectroscopy (STS) is able to probe the conductance which is proportional to local density of states (LDOS) of sample within the small bias range [39-40]. The conductance mapping image thus represents the contour map of surface LDOS at a certain bias voltage. As for the spin-resolved tunneling spectroscopy (SP-STS), it is another important operation mode in the SP-STM technique. Similar to the STS in the application of distinguishing different chemical elements or local electronic changes on the surface, the SP-STS can be applied to separate topographic, electronic and magnetic information in the SP-STM experiements. In the SP-STS measurements on the Gd(0001) by Bode *et al.* [41], due to the exchange splitting, both the majority and minority components of the Gd(0001) surface state appear within the bias range of ± 1.0 Vin the tunneling spectra. Therefore, the majority spins from spin-polarized probe will be parallel to the majority spins and antiparallel to the minority spins from Gd(0001) surface states. As a consequence, the spin-resolved tunneling conductance will enhance and reduce for the situations of parallel and

antiparallel, respectively. Since the coercivity of freestanding Gd islands on W(110) is small, the spin-polarized vacuum tunneling into the exchange-split surface state of Gd(0001) has been demonstrated in the applied external field. This experiement indicates the magnetic effect could be distiguished by the SP-STS spectra in the systems with both exchange-split surface states nearby the Fermi level. This case is not general in many other magnetic systems and only one or even not existence of spin-polarized surface state nearby the Fermi energy level are the most common circumstances. Instead of spin-polarized tunneling into exchange-split surface states, however, the magnetization switching of tip or sample in the SP-STM experiments is more reliable way to extract magnetic signals and versatile in the application of complicated magnetic systems. The external applied magnetic field is obviously one of the solutions and has been employed to achieve such purpose on switching magnetization of either spin-polarized tip or magnetic sample in SP-STM experiments [42-44].

2.3 Coil wound CoFeSiB tip

The soft magnetic tip with a small coil wound around has been applied to the SP-STM technique by Wulfhekel and Kirschner *et al.* [45]. As shown in the Fig. 3, two different tip geometries have been developed for the in-plane or out-of- plane spin sensitivity [46, 47]. In this method, the operation mode with the employment of such kind of tip can be also applied to separate magnetic from electronic or topographic contributions and magnetization direction of tip is defined according to different geometry of designed tip shape. In combination with the technique of lock-in amplifier, a small and high frequency bias voltage is applied to modulate the tip magnetization switching periodically through the wound coil. In analogy to earlier experiment [48], a tiny coil is also used to switch nickel tip magnetization back and forth in the stationary spin-polarized tunneling measurements. Due to the switching frequency is much higher than the cut-off frequency of STM feedback loop, there is no any mechanical response from STM operated in constant current mode. Thus, the periodical switching of the tip magnetization causes an additional ac tunneling current based on the tunneling magnetoresistance (TMR) effect [30]. This ac tunneling current is sensitive to the magnetization orientation on the sample surface according to the derivation of dI/ dm_T is proportional to m_S from Wortmann et al. [31], where the m_T and m_S are the magnetization DOS of tip and sample, respectively. By using the phase sensitive lock-in amplifier, this corresponding ac tunneling current can be measured. Because of the well-defined switching magnetization direction of tip in this method, the in-plane complex surface spin configurations can be also mapped out by rotating 90 degree of tip magnetization direction to the other orthogonal in-plane direction [49]. Furthermore, due to this approach only detects the magnetization DOS of sample, the application in the resolving spin structures of magnetic alloy system with different chemical species has been demonstrated [50].

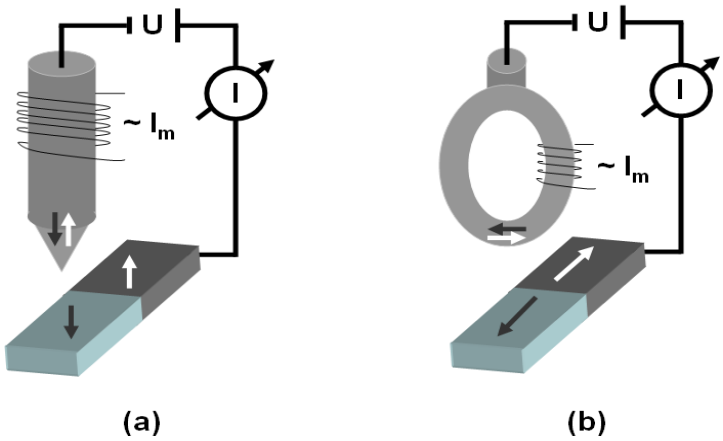

Fig. 3 Schematic representation of different tip geometry shapes in modulated tip magnetization mode of SP-STM. The CoFeSiB tips with different geometries are made by lithography process and chemical etching. After that, a small coil is wound on the designed CoFeSiB tip. By utilizing the magnetic shape anisotropy, for the most front tip end atoms with the out-of-plane spin sensitivity is shown in (a) and with the in-plane spin sensitivity is in (b).

The material choosed for the tip magnetization switching driven by small bias voltage is an amorphous metallic glass of CoFeSiB. The low magnetostriction can avoid vibrations of the tip during switching of its magnetization. Further, the low coercivity and saturation magnetization minimize the magnetization losses during the tip magnetization switching and reduce the stray field from tip as well. However, the preparation of such tips is a non-trivial task and time consuming, including lithography procedures, chemical etching and small coil winding. In addition, the spin-polarization of magnetic sample is not constant over the range of scanning bias voltages, it is possible to obtain vanished dI/ dm_T signal at a cerain bias voltage even the fact that the local sample magnetization still exists. This can be verified in the SP-STS measurements on the bias dependence of spin-polarized tunneling current in this method [51]. Another difficulty of this method is the application in the low temperature. One of the apparent difficulties is that the coercive field will become larger while the tip is placed into the environment of low temperature. To overcome this, either the number of cycles of the small coil or the bias voltage driving tip magnetization switching has to be increased. Until present, the SP-STM technique operated at this mode only has been applied to the room temperature experiements and the experiements carried out at the low termperature have not been reported yet.

3. In-plane spin sensitive magnetically coated ring-shaped tip

3.1 Atomic resolution resolved by ring-shaped tip in STM

In respect to the tip shape geometry designed for in-plane spin sensitivity in the modulated tip magnetization mode, the ring-shaped probe simply made by bending the tungsten wire has been created by C.-B. Wu and M.-T. Lin *et al.* [52]. Before introducing the ring-shaped tip into the SP-STM technique, preliminary studies of this kind of tip in the application of STM scanning will be discussed. The preparation of ring-shaped tip is relatively easier as compared to the previous methods including the lithography processes, chemical etching, and mechanical polishing etc. As shown in the Fig. 4(a), the tungsten wire with a diameter around 50 μm is simply bended into a ring-shaped probe and mounted into the tip carrier as the usual sharp tungsten tip. After transferring it into the UHV chamber, further step has to be taken to remove the oxide and carbon contanminated layers of the front tip end. There are some typical approaches, e.g., electron bombardment, ion sputtering, field emission etc, developed to *in situ* clean the tip. This procedure is very important in the SP-STM technique because the contanmination can greatly reduce the spin polarization and affect the magnetic properties of the spin-polarized tips. Therefore, finding a good and reliable procedure to have tip cleaned plays important role in realizing the successful vacuum spin-polarized electron tunnelling in SP-STM.

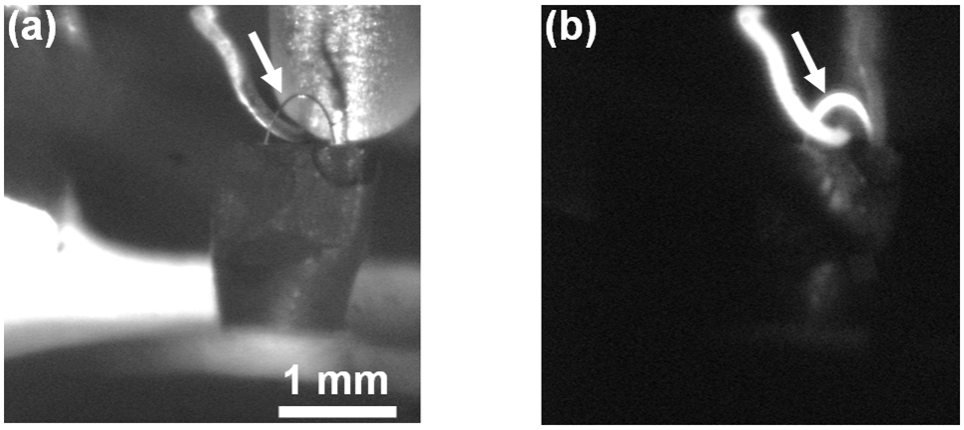

Fig. 4 The ring-shaped tip probe simply made by bending tungsten wire and mounted in the tip carrier is shown in the (a). Same ring-shaped tip is annealed by direct current heating method in (b). Part of front tip end is incandescent due to the high temperature able to be reached during the heating. The white arrow indicates the ring-shaped tip in the both insets.

Directly passing the current through the part of front ring-shaped tip end is our method to heat it up. There are another two isolated tungsten rods with larger diameter of around 380 μm and the ring-shaped tip can electrically bridge them together. Then the current is passed from one to the other rod forming a complete current loop. Due to the higher electric resistance of the ring-shaped tip with smaller diameter of tungsten wire, the effect of resistive heating is achieved in this setup. As shown in the Fig. 4(b), the ring-shaped tip directly contacts with two isolated tungsten rods and is incandescent while the high temperature has been reached. Besides the observation from naked eyes, the SEM images before and after annealing the ring-shaped tip have been demonstrated in the Fig. 5.

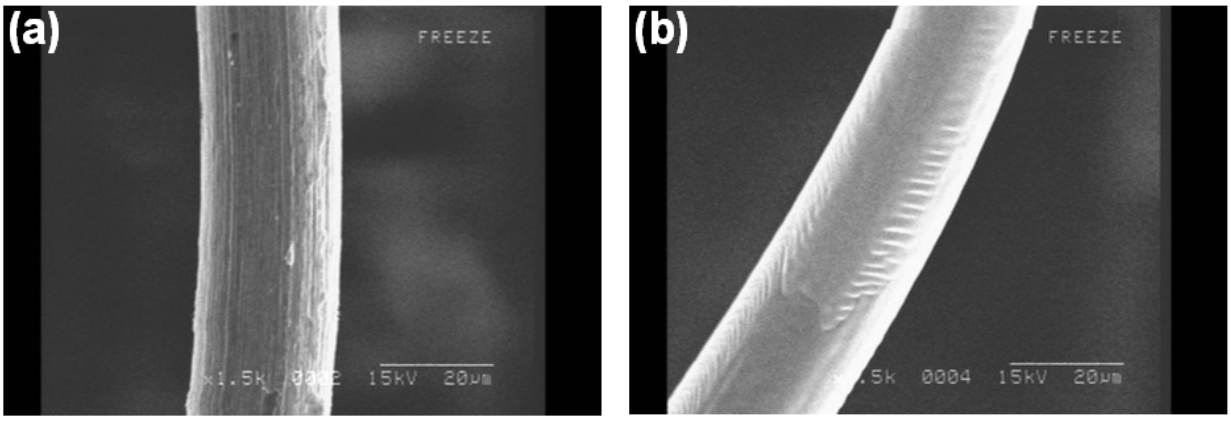

Fig. 5 The SEM image of ring-shaped tip probe before the annealing by means of current direct heating is shown in (a). As observed from the image, the surface of ring-shaped tip is rough and has line scratch pattern. On the contrary, after annealing, the smooth surface and even the ripple from the melting of tungsten wire can be indicated in the (b). This demonstrates the direct heating method capable of *in situ* heating the ring-shaped tip up to high temperature and cleaning the front tip end very well.

The clean ring-shaped tip has been applied to the STM scanned at the room termperature and the spatial resolution down to atomic scale can be achieved. In spite of macroscopic blunt of the tip, the atomic resolution images of different substrates have been resolved and shown in the Fig. 6. This is because the tunnelling current only dominated by the most front few atoms of the tip and there are actually many mini tips created in the microscopic point of view of the

front ring-shaped tip end. In addition, the stable STM and quiet environment are also important for the atomic scale resolution and measurements. The fresh surface of highly oriented polycrystalline graphite (HOPG) substrate is prepared by pressing a piece of double-stick tape to the HOPG surface and then gently peeling it off the surface. Repeat the above surface peeling procedure until the HOPG surface appears to be flat to the naked eyes. Then mount the HOPG on the sample plate and transfer it to the UHV champer as soon as possible. The atomic resolution image of HOPG is shown in the Fig. 6(a). The corresponding fourier transform pattern (not shown here) is not perfect hexagonal symmetry, but with a elongation along y direction. By calibrating the piezo scanner properly, the distorted topography images will restore to perfect hexagonal lattice with proper length. Besides the HOPG atomic resolution can be achieved by the ring-shaped tip, it is also applied to the Si(111) 7x7 superstructure and Cu(001) surface. The Si(111) 7x7 superstructure can only be prepared and measured in UHV condition. There are some bright spots on the surface shown in the Fig. 6(b) and the number of density will slowly increase with the scanning time. In our speculation, these might be the silicon oxides from residual gas in the UHV chamber even at the pressure of ~ $1x10^{-10}$ mbar. The last one is the atomic resolution image obtained on the clean Cu(001) substrate. From the image shown in the Fig. 6(c), clearly copper atoms arrangement can be seen and one surface defect is at the upper right corner of image.

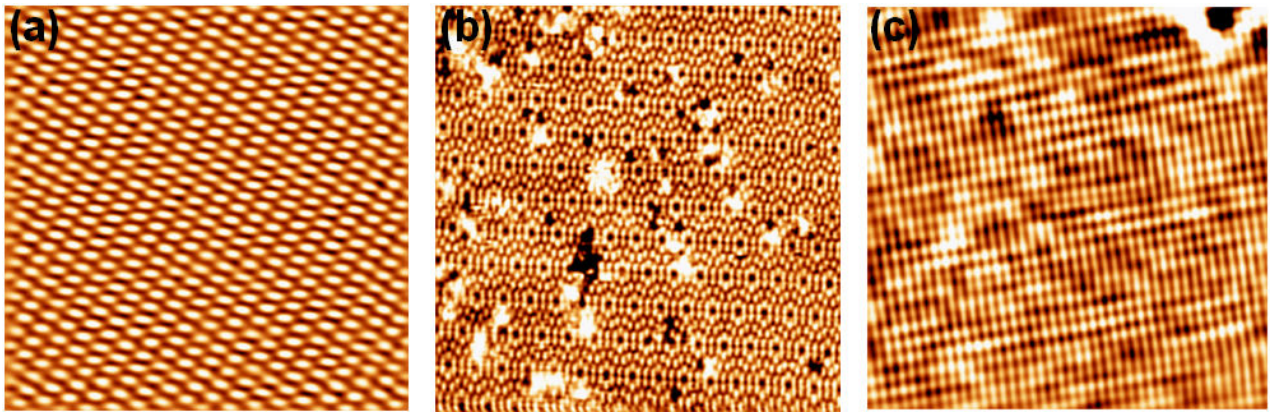

Fig. 6 The STM atomic resolution images on different substrates resolved by using ring-shaped tip. (a) Highly oriented polycrystalline graphite (HOPG) substrate, U= 0.3 V, I= 3 nA, 5 nm x 5 nm. (b) Si(111) 7x7 superstructure prepared by flash annealing method, U= 1.5 V, I= 0.5 nA, 40 nm x 40 nm. (c) Cu(001) substrate, U= 1.5 V, I= 0.5 nA, 10 nm x 10 nm.

3.2 Magnetically coated ring-shaped tip applied to SP-STM

According to the spin dependent tunnelling theory, the TMR effect is proportional to cos(θ), in which θ is the angle between the respective magnetization of the two ferromagnetic electrodes. In addition, by using the geometry of a ring-shaped tip, the magnetization of coated magnetic materials should be along the surface in-plane direction due to magnetic shape anisotropy, such that the magnetically coated ring-shaped tip should be sensitive to in-plane component of spins and hence be able to map out the in-plane spin projections of magnetic spin structures in the application of SP-STM technique [52]. In order to verify the magnetic propery of 20 monolayers (MLs) Fe coated ring-shaped probe, it is capped with several monolayers of Cu and MOKE measurement at ambient conditions are performed. With the laser beam focused on the leading edge of the ring, the hysteresis loop for the field applied parallel to the ring plane is measured and shown in Fig. 7(c). One can clearly observe a square hysteresis loop with coercivity around 80 Oe[52]. This indicates that the probe magnetization with the help of shape anisotropy can be easily stabilized along the ring periphery after applying saturating field. As a result, it can serve as a spin-sensitive probe for mapping out the in-plane domain structure of the sample.

We choose Mn/ Fe (001) as the test system because Mn exhibits layer-wise antiferromagnetism when the thickness is larger than 3 ML [53-55], and its spin direction is determined by the ferromagnetic iron whisker substrate, whose dimension is 2 mm wide and 10 mm long, preferring the magnetization parallel to the long axis. The whole experiment is conducted in an ultrahigh vacuum chamber whose base pressure is < 2 x 10^{-10} mbar and equipped with various thin film deposition and characterization tools [56]. The Fe(001) substrate is cleaned by cycles of sputtering and annealing until a clear low energy electron diffraction pattern can be observed. After that, the routine process is to sputter the substrate for 1 h at room temperature and then at 1000 K for another half hour, followed by cooling to 400 K and depositing Mn film on it at the same temperature with the deposition rate around 1.5 ML/min. After the deposition, the sample is transferred to the STM chamber, inside which the STM and STS experiments are performed at room temperature with the field aligned magnetic ring probe prepared by the method mentioned above. In the spectroscopy mode, 101 data points of tunneling current from a bias voltage of −0.5 ~ +0.5 V are taken at each pixel with feedback loop open, and numerically differentiated to get the conductance spectra.

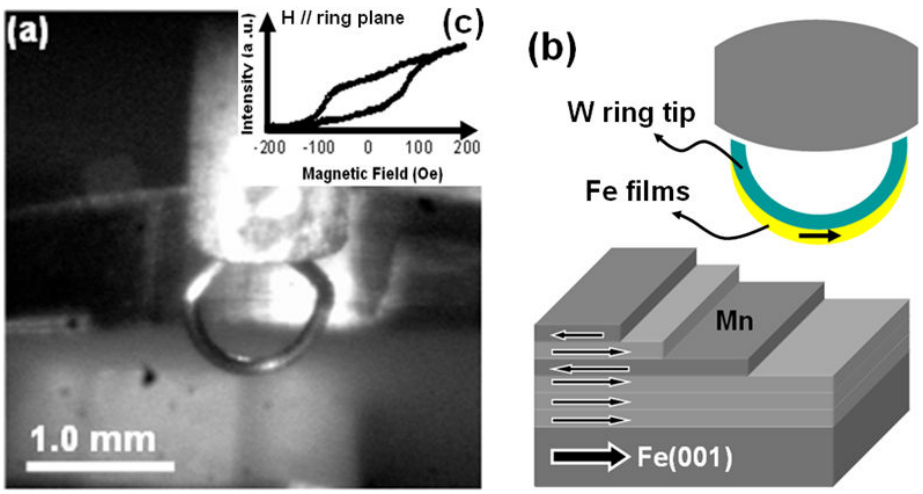

Fig. 7 (a) Photography of the ring probe made of 125 μm wide tungsten wire, (b) schematics of parallel magnetizations of the sample and the iron films coated on the ring-shaped tip, and (c) Kerr hysteresis loop for the magnetic field (H) applied parallel to the ring plane [52].

The topography of 6.8 ML Mn/ Fe(001) is shown in Fig. 8(a) in which the scanning parameters of sample bias voltage and feedback current are of 1V and 0.1 nA, respectively [52]. The Mn films have a layer-by-layer growth mode on the Fe(001) so that we can observe the sixth and seventh layers on the surface. The interlayer distance is measured to be 0.19 ± 0.03 nm from the line profile shown in Fig. 8(c). The current map resolved by Fe coated ring-shaped tip of the same area at +0.5 V is also shown in Fig. 8(b). Contrast between the sixth and seventh layers can be observed in the current map, which is further justified by the line profiles of topography and current map at the same place in Fig. 8(c). The seventh layer has current of about 5 % higher than the sixth layer. Since there is no chemical difference between these two Mn layers, the contrast can only originate from the spin difference. The spin-dependent DOS results in the different I(U) curves of the parallel and antiparallel configurations according to the spin dependent tunneling. The averaged I-U spectra of the sixth and seventh layers are shown in Fig. 8(d). It is observed that the seventh layer has slightly higher current all the way from 0 to +0.5 V than the sixth layer. To see the difference clearer, the numerically differentiated tunneling conductance spectra are shown in the same figure. We note that the conductance of positive bias voltage is higher than that of negative bias, which reflects the difference between the unoccupied and occupied densities of states of the sample. Furthermore, the conductance increases almost linearly with bias voltage from 0 to +0.4 V, and then rises with steep slope. This trend could be decomposed into an exponential background plus a surface state peak, as pointed out by Bischoff et al. in Ref. 57. These spin-polarized surface states can enhance the contrast in the current map. Even though it looks macroscopically blunt, the spatial resolution of the ring probe made by this simple method is not a problem in this system. Actually, since it is the atom at the very end of the probe which contributes overwhelming proportion of the tunneling current, even a blunt tip can give spatial resolution down to the nanometer scale if the sample is flat enough [49], which is exactly the case for Mn thin films on iron whisker. The atomic step edge is resolved to be within 2 nm in Fig. 8(c).

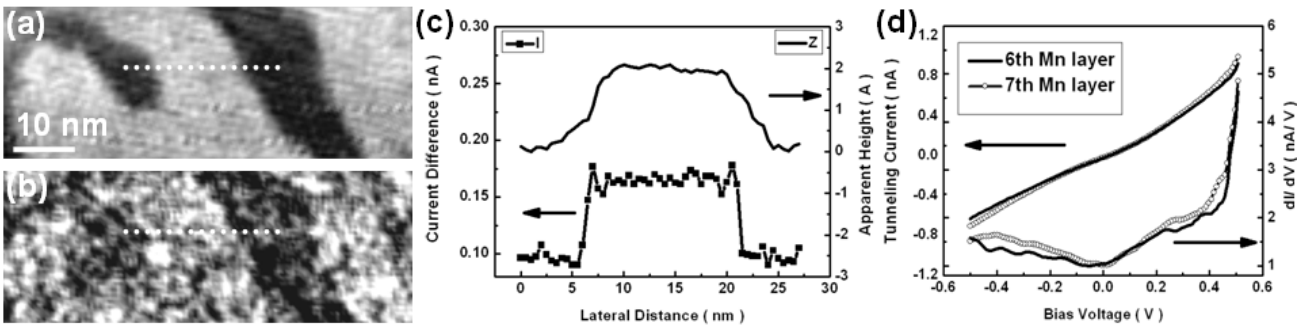

Fig. 8 (a) STM constant current image of 6.8 ML Mn/ Fe(001) with feedback parameters of U= +0.1 V, I= 0.1 nA, and (b) its current map at +0.5 V. Line profiles along the black dashed lines in (a) and (b) are shown in (c). (d) I-U spectra, averaged over the sixth and seventh layers, respectively, with their numerically differentiated conductance spectra shown in the lower part [52].

4. *In situ* out-of-plane magnetization switching of magnetic probe tip

In addition to the in-plane spin sensitivity achieved by using a magnetically coated ring-shaped tip, the *in situ* out-of-plane magnetization switching of a magnetic probe is also realized through the magnetic interactions between tip and

sample by P.-J. Hsu and M.-T. Lin *et al.* [59]. As mentioned in above section, one of the important issues on spin-polarized tips designed for SP-STM experiments[37, 60] is to separate the magnetic from topographic and chemical contributions to the tunneling current. The magnetization direction switching of either the sample or the tip has the opportunity to fulfill such a purpose. As reported by the previous SP-STM experiments [42-44], owing to the fact that both sample and tip were under strong external magnetic field, magnetization direction rotation needed to be carefully controlled to ensure magnetization switching of sample or tip only. Instead of applying external magnetic field, recent theoretical studies also reported that varying tip-substrate distance was applicable in order to switch a single spin through the competition of direct and indirect exchange coupling [61-63]. In light of this, soft magnetic materials with low coercivity field for are an appropriate candidate for a spin-polarized probe, offering *in situ* magnetization switching in the SP-STM technique.

The soft magnetic tip from an FeMnC alloy material has been applied to be the spin-polarized probe with out-of-plane spin sensitivity for the Co nanoislands grown on Cu (111) with out-of-plane magnetization [64, 65]. Most importantly, in order to have magnetic signals distinguished, an *in situ* switching of the tip magnetization direction can be achieved through varying tip-substrate distance, revealing the magnetic domain of Co nanoislands with reversed spin contrast. The experiment was carried out in a UHV chamber with base pressure of around $3x10^{-11}$ mbar. The Cu(111) substrate was cleaned by cycles of 1 keV Ar^+ sputtering and annealing at 850 K. After that, submonolayer Co was evaporated on the Cu(111) at room temperature through molecular beam epitaxy technique with a deposition rate of 0.6 ML min^{-1} calibrated from STM. After sample preparation, it was subsequently transferred into a low temperature STM cooled to 4.5 K with pressure of around $2x10^{-12}$ mbar.

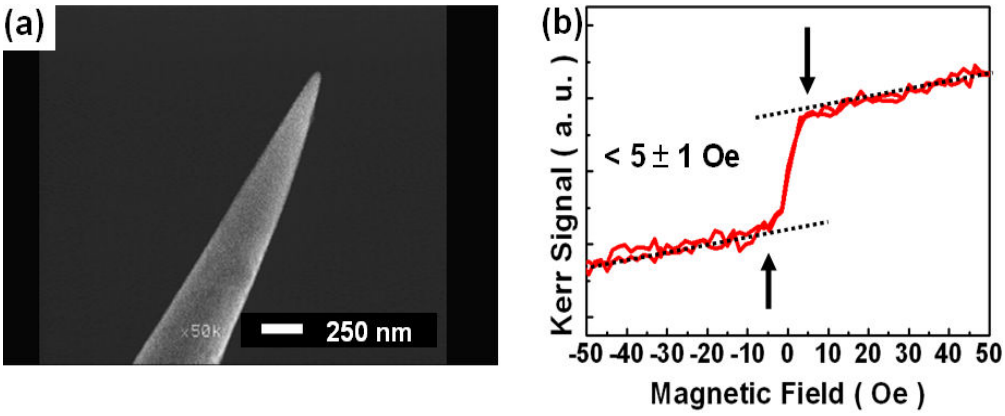

Fig. 9 (a) Magnified image of soft magnetic tip is taken by the SEM. (b) Magnetic hysteresis loop of FeMnC alloy tip from the MOKE measurements and the switching field smaller than 5 ± 1 Oe can be characterized [59].

The tip probe of FeMnC alloy material was first prepared by mechanical milling and the corresponding magnetic properties were checked with the MOKE measurements. The tip image taken from SEM is shown in the Fig. 9(a). In addition, as shown in the Fig. 9(b), the small coercivity and switching field around 5 ± 1 Oe can be characterized from the magnetic hysteresis loop. After the tip was transferred into UHV chamber, it was further sputtered by 3 KeV Ar^+ ion bombardment. Furthermore, in order to improve the spin contrast [46, 47], but retain a low coercivity necessary for the ease of magnetization switching, a few monolayers of Co was deposited. The magnetic stability was verified in such Co coated tip at regular tunneling distance, to ensure that they can be applied to SP-STS measurements with reliability. As for the tunneling spectroscopy measurements, the feedback loop was open and the sample bias ramped from +1.0 to -1.0 V whereas the distance between the tip and sample was stabilized typically at scanning parameters of +1.0 V and 1.0 nA. The differential conductance spectra were recorded simultaneously to the topographic images by adding a voltage modulation of 20 mV_{rms} to the sample bias and detecting the signals by the lock-in technique.

A typical STM topography of 0.35 ML Co grown on Cu(111) is shown in Fig. 10(a). There are two kinds of Co nanoisland arrangements, namely faulted and unfaulted fcc stackings, protruding with bilayer height from the Cu surface [66, 67]. By using the magnetic tip, the spin-polarized conductance mapping resolved at bias of -316 mV and -494 mV are presented in Figs. 10(b) and 10(c), respectively. In order to prevent the influence from crystalline and size dependent peak position of surface state [64, 68], we discuss the conductance curves on Co nanoislands with equal stackings and sizes, as the two sets of them marked from A to D in the Figs. 10(b) and 10(c). And their corresponding conductance curves depicted with different colors are shown in top of Fig. 10(d). The prominent surface state peak of the conductance curve at around -0.31 V is consistent with previous studies [64, 67] and contributes to the significant spin-polarization amplitude due to the hybridization of *s-p* states with the minority $d_{3z^2-r^2}$ band of Co nanoislands. The structural and magnetic asymmetry curves defined as [37, 64]

$$A_{structral} = \frac{dI/dU_{unfaulted\uparrow\uparrow(\downarrow)} - dI/dU_{faulted\uparrow\uparrow(\downarrow)}}{dI/dU_{unfaulted\uparrow\uparrow(\downarrow)} + dI/dU_{faulted\uparrow\uparrow(\downarrow)}}, \quad A_{magnetic} = \frac{dI/dU_{(un)faulted\uparrow\uparrow} - dI/dU_{(un)faulted\uparrow\downarrow}}{dI/dU_{(un)faulted\uparrow\uparrow} + dI/dU_{(un)faulted\uparrow\downarrow}}.$$

respectively, are shown in the bottom of Fig. 10(d). The conductance curves from these two different derivations can thus be clearly distinguished. Besides, the characteristic oscillatory behavior of magnetic asymmetry due to the sign reversal of spin polarization is also observed, being consistent with previous studies [64].

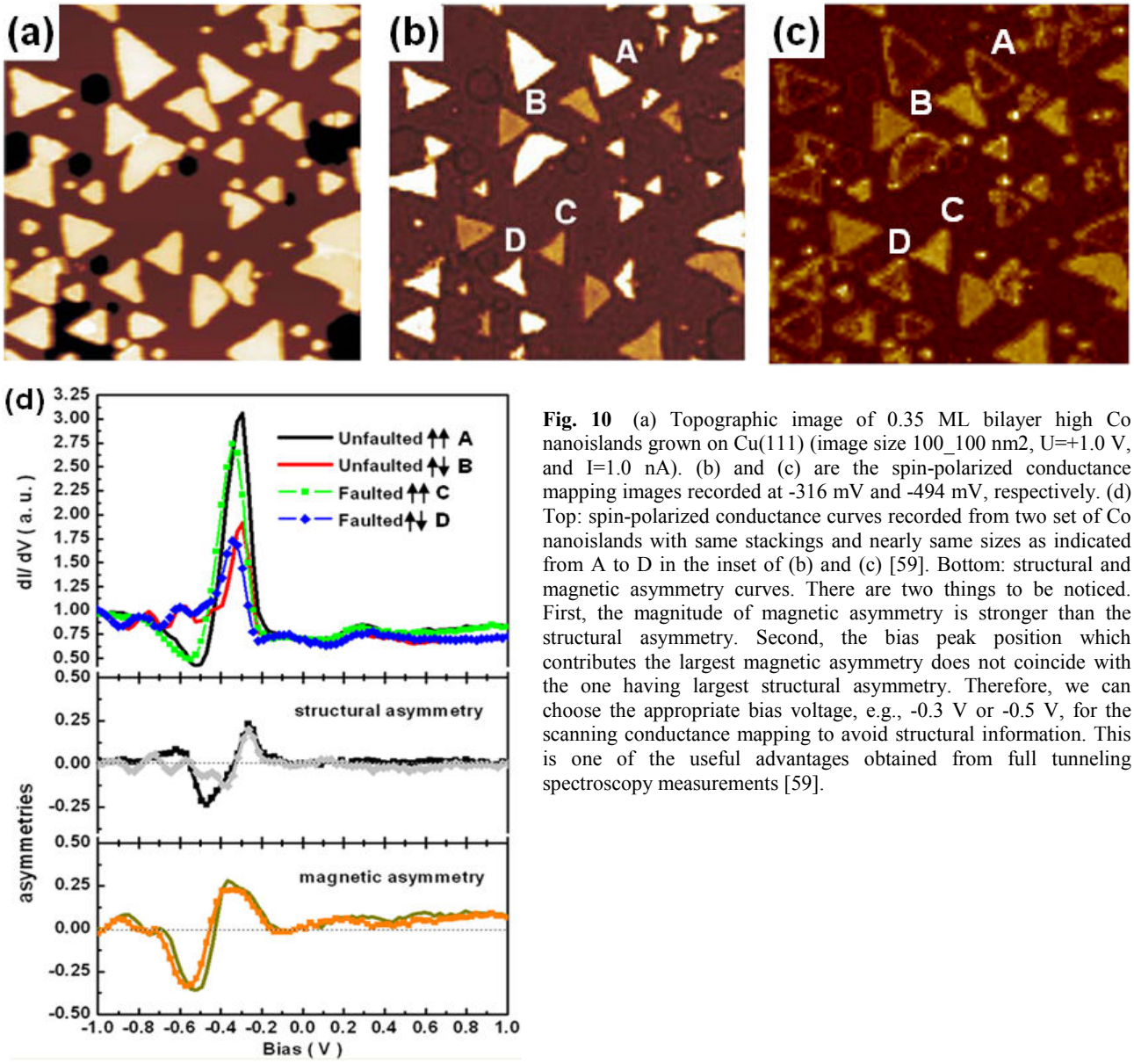

Fig. 10 (a) Topographic image of 0.35 ML bilayer high Co nanoislands grown on Cu(111) (image size 100_100 nm2, U=+1.0 V, and I=1.0 nA). (b) and (c) are the spin-polarized conductance mapping images recorded at -316 mV and -494 mV, respectively. (d) Top: spin-polarized conductance curves recorded from two set of Co nanoislands with same stackings and nearly same sizes as indicated from A to D in the inset of (b) and (c) [59]. Bottom: structural and magnetic asymmetry curves. There are two things to be noticed. First, the magnitude of magnetic asymmetry is stronger than the structural asymmetry. Second, the bias peak position which contributes the largest magnetic asymmetry does not coincide with the one having largest structural asymmetry. Therefore, we can choose the appropriate bias voltage, e.g., -0.3 V or -0.5 V, for the scanning conductance mapping to avoid structural information. This is one of the useful advantages obtained from full tunneling spectroscopy measurements [59].

After the magnetic domain images and spin-polarized conductance spectra have been resolved, the reversal spin contrasts recorded at a bias of -0.3 V and 1.0 nA are sequentially shown in Figs. 11(a) to (c). At first, the topography of 0.66 ML Co nanoislands and the spin-polarized conductance mapping, recorded simultaneously, are shown in the inset of Fig. 11(a) and Fig. 11(a), respectively. The spin contrast of these nanoislands can be clearly observed according to the magnetization direction parallel or antiparallel to that of the magnetic tip [30]. Besides the spin contrast, some black spots on the surface of Co nanoislands are also observed due to the segregation of Cu atoms [69]. Afterward we move the tip to one of Co nanoislands, as shown by F in the Fig. 11(a), with the magnetization antiparallel to the tip magnetization, and decrease the tip-substrate distance by reducing the bias to 3 mV and increasing the current to 30 nA, which is much smaller than the current used in the spin injection of previous SP-STM experiments [70]. The corresponding conductance is ~$0.258G_0$, where $G_0 \equiv e^2/h$ is for two magnetic electrodes without spin degeneracy [71, 72]. After that, we go back to the normal scanning parameters of -0.3 V and 1.0 nA, and the reversal spin contrast of all Co islands can be clearly observed in the Fig. 11(b). By repeating this process at another Co nanoisland E' of Fig. 11(b), we can reverse again the spin contrast images as shown in the Fig. 11(c) similar to the Fig. 11(a). This demonstrates that the magnetization direction of tip end can be reversed back by such an operation. In addition, for the segregated Cu atoms, i.e., black spots on the surface of Co nanoislands in the spin contrast images, there is no contrast between them

during the magnetization switchings of tip end. Separation of magnetic signal from topographic or chemical contributions could thus be achieved in such way.

The tunneling spectroscopy measurements before and after tip magnetization switchings are also presented in the Fig. 11(d). From the comparison of spin-polarized conductance curves of E and F taken from Co nanoislands indicated in the Fig. 11(a), it is seen that curve E has stronger amplitude than curve F at around -0.3 V and to the contrary, curve F has stronger amplitude than curve E at around -0.5 V. Such behavior reverses in the curves of E' and F' due to the magnetization switching of the tip apex and reverses back again in the curves of E'' and F''. Besides, from the asymmetry curves illustrated in the Fig. 11(d), the main contribution to spin contrast reversal are indicated by the arrows in the bias voltage region of spin-polarized surface state. The slight difference in the asymmetry curves, especially at around -0.7 V (Ref. 64) which is not reversed accordingly, might come from the complex intra-atomic noncollinear magnetism of the magnetic tip end [73] and requires further studies in the future. Nevertheless, the tip magnetization switching behavior is much clearer and can be identified from the pronounced spin-polarized surface state at around -0.3 V.

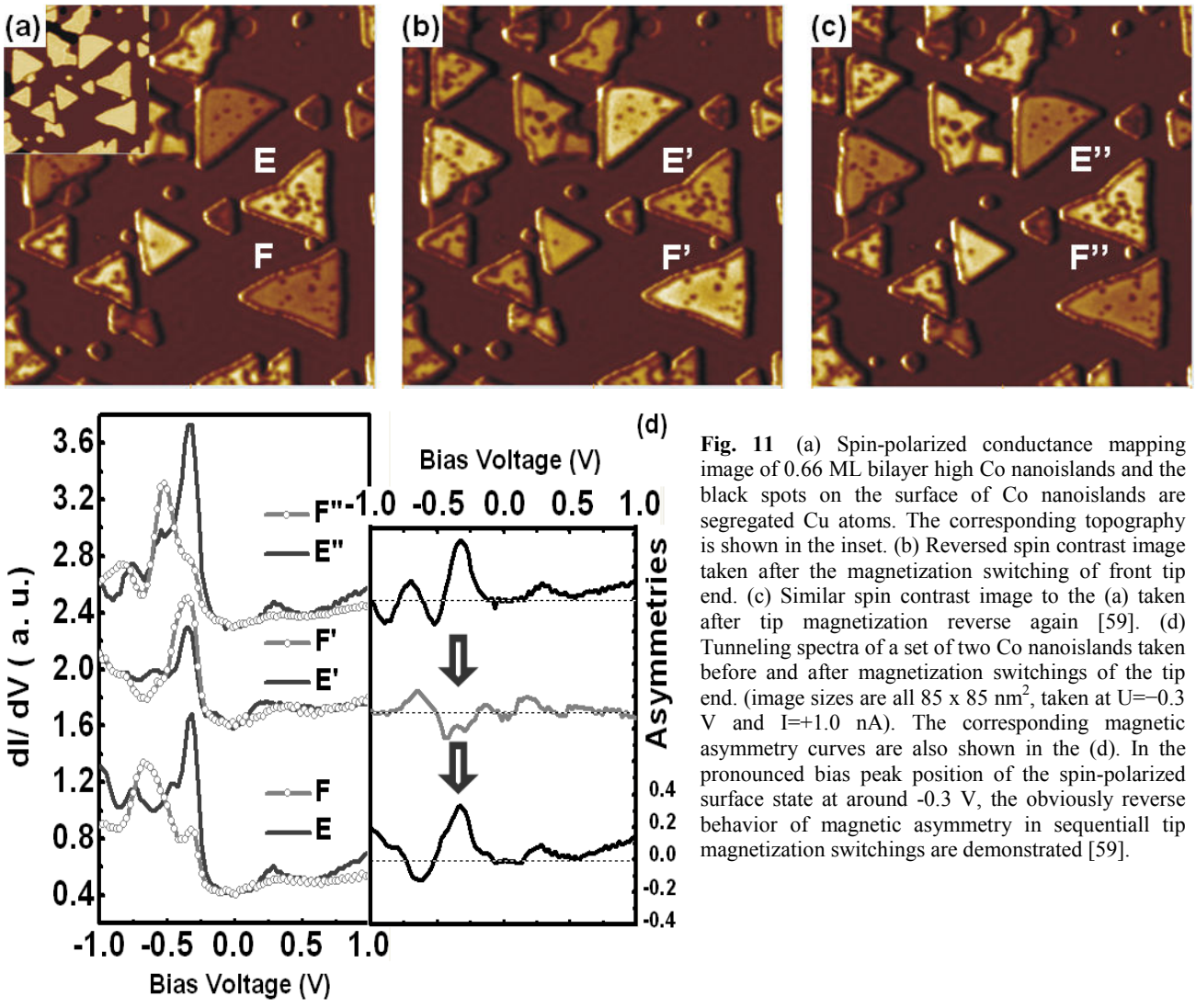

Fig. 11 (a) Spin-polarized conductance mapping image of 0.66 ML bilayer high Co nanoislands and the black spots on the surface of Co nanoislands are segregated Cu atoms. The corresponding topography is shown in the inset. (b) Reversed spin contrast image taken after the magnetization switching of front tip end. (c) Similar spin contrast image to the (a) taken after tip magnetization reverse again [59]. (d) Tunneling spectra of a set of two Co nanoislands taken before and after magnetization switchings of the tip end. (image sizes are all 85 x 85 nm^2, taken at U=−0.3 V and I=+1.0 nA). The corresponding magnetic asymmetry curves are also shown in the (d). In the pronounced bias peak position of the spin-polarized surface state at around -0.3 V, the obviously reverse behavior of magnetic asymmetry in sequentiall tip magnetization switchings are demonstrated [59].

5. Summary

Magnetic shape anisotropy plays the most important role in determining the magnetization direction of spin-polarized probes. The success of obtaining spin contrast demonstrates the capability of a tungsten ring probe made by bending a fine tungsten wire with magnetical coating. Such probe is easy to prepare without highly demanding procedures. After the magnetization of the probe is saturated by an external field, it can give a well defined in-plane magnetization direction of the coated ferromagnetic thin film, and thus can be applied to image magnetic domain structures with spin sensitivity in a specific in-plane direction down to nanometer scale. In addition to the in-plane magnetization control

using a magnetically coated ring-shaped tip, the FeMnC alloy material with low coercivity field has also been applied as the spin-polarized probe with the capability of *in situ* out-of-plane magnetization direction switching. According to the consequential reversal spin contrast of Co nanoislands, tip magnetization switching can be achieved through reducing tip-substrate distance. Instead of changing tip end spin structures by transferring atoms onto the sample surface in the approach of point contact [74], the magnetic interactions between tip and sample can also give rise to magnetization switchings of magnetic probes. Moreover, in combination with the SP-STS measurements before and after tip magnetization switchings, the sequential reversals of magnetic asymmetries at the bias peak position of pronounced spin-polarized surface state indicate the credible tip magnetization switchings as well. This provides an effective method not only for distinguishing magnetic signals from chemical or topographic contributions without applying external magnetic field, but also the capability of studying complex magnetic spin structures with various nonmagnetic impurities or compositions involved in the SP-STM.

Acknowledgements We would like to thank C. B. Wu, H. Y. Yen, C. I. Lu, S. W. Chen, W. J. Hsueh, Y. H. Chu, C. H. Hsu, and C. J. Butler for their valuable contributions in this work and acknowledge the financial support from National Science Council of Taiwan under Grant Nos. NSC 98-2120-M-002-010, NSC 96-2120-M-002-011 and NSC 95-2112-M-002-051-MY3.

References

[1] A. Hubert, and R. Schäfer, Magnetic Domains: The Analysis of Magnetic Microstructures. Springer-Verlag Berlin Heidelberg (1998).
[2] F. Bitter, Phys. Rev. 41, 507 (1932).
[3] A. Hubert, Phys. Status Solidi. 24, 669 (1967).
[4] Y. Martin and H. K. Wickramasinghe, Appl. Phys. Lett. 50, 1455 (1987).
[5] U. Hartmann, T. Göddenhenrich, C. Heiden, J. Magn. Magn. Mat. 101, 263 (1991).
[6] M. Dreyer, M. Kleiber, A. Wadas, and R. Wiesendanger, Phys. Rev. B 50, 4273 (1999).
[7] H. J. Williams, F. G. Foster, and E. A. Wood, Phys. Rev. B 82, 119 (1951)
[8] S. D. Bader, E. R. Moog, and P. Grunberg, J. Magn. Magn. Mat. 53, L295 (1986).
[9] C. Durkan, I. V. Shvets, and J. C. Lodder, Appl. Phys. Lett. 70, 1323 (1997)
[10] E. Betzig, J. K. Trautmann, R. Wolfe, E. M. Gyorgy, and P. L. Flinn, Appl. Phys. Lett. 61, 142 (1992)
[11] P. R. Aitchison, J. N. Chapman, V. Gehanno, I. S. Weir, M. R. Scheinfein, S. McVitie, and A. Marty, J. Magn. Magn. Mater. 223, 138 (2001)
[12] K. Koike, H. Matsuyama, H. Todokoro, and K. Hayakawa, Scanning Microscopy 1, 31 (1987).
[13] J. Unguris, M. R. Scheinfein, M. H. Kelley, A. Gavrin, R. J. Celotta, and D. T. Pierce, in Handbook of Microscopy, VCH Verlagsqesellschaft, 735-749 (1997).
[14] J. Kirschner, in: A. Howie, and U. Valdé, Surface and Interface Characterization by Electron Optical Methods, New York, London, Plenum Press (1998).
[15] E. Bauer, in: H. Hopster, and H. P. Oepen, Magnetic Microscopy of Nanostructures, Springer-Verlag Berlin Heidelberg (2005).
[16] W. Kuch, J. Gilles, S. S. Kang, S. Imada, S. Suga, and J. Kirschner, Phys. Rev. Lett. 62, 3284 (2000)
[17] F. Nolting, A. Scholl, J. Stöhr, J.W. Seo, J. Fompeyrine, H. Siegwart, J.-P. Louquet, S. Anders, J. Lünig, E.E. Fullerton, M.F. Toney, M.R. Scheinfein, and H.A. Padmore, Nature 405, 767 (2000).
[18] G. Binning, H. Rohrer, Ch. Gerber, and E. Weibel, Phys. Rev. Lett. 49, 57 (1982).
[19] P. M. Tedrow, and R. Meservey, Phys. Rev. B 7, 318 (1973)
[20] D.T. Pierce, Physica Scripta 38, 291 (1988).
[21] S. F. Alvarado, and P. Renaud, Phys. Rev. Lett. 68, 1387 (1992).
[22] S. F. Alvarado, Phys. Rev. Lett. 75, 513 (1995).
[23] Y. Suzuki, W. Nabhan, and K. Tanaka, Appl. Phys. Lett. 71, 3153 (1997).
[24] A. L. Vásquez de Parga, and S. F. Alvarado, Europhys. Lett. 36, 577 (1996)
[25] V. P. LaBella, D. W. Bullock, Z. Ding, C. Emery, A. Venkatesan, W. F. Oliver, G. J. Salamo, P. M. Thibado, and M. Mortazavi, Science 292, 1518 (2001).
[26] W. F. Egelhoff, Jr., M. D. Stiles, D. P. Pappas, D. T. Pierce, J. M. Byers, M. B. Johnson, B. T. Jonker, S. F. Alvarado, J. F. Gregg, J. A. C. Bland, R. A. Buhrman, V. P. LaBella, D. W. Bullock, Z. Ding, C. Emery, A. Venkatesan, W. F. Oliver, G. J. Salamo, P. M. Thibado, and M. Mortazavi, Science **296,** 1195 (2002).
[27] R. Wiesendanger, H.-J. Güntherodt, G. Güntherodt, R.J. Gambino, and R. Ruf, Phys. Rev. Lett. **65**, 247 (1990).
[28] S. Blügel, D. Pescia, and P. H. Dederichs, Phys. Rev. B **39,** 1392 (1989).
[29] R. Wiesendanger, I.V. Shvets, D. Bürgler, G. Tarrach, H.-J. Güntherrodt, J.M.D. Coey, and S. Gräser, Science **255**, 583 (1992).
[30] M. Julliere, Phys. Lett. A **54**, 225 (1975).
[31] D. Wortmann, S. Heinze, Ph. Kurz, G. Bihlmayer, and S. Blügel, Phys. Rev. Lett. **86**, 4132 (2001).
[32] S. Heinze, M. Bode, A. Kubetzka, O. Pietzsch, X. Nie, S. Blügel, and R. Wiesendanger, Science **288**, 1805 (2000).
[33] H. Yang, A. R. Smith, M. Prikhodko, and W. R. L. Lambrecht, Phys. Rev. Lett. **89**, 226101 (2002).
[34] N. Berdunov, S. Murphy, G. Mariotto, and I. Shvets, Phys. Rev. Lett. **93**, 057201 (2004).
[35] M. Bode, M. Heide, K. von Bergmann, P. Ferriani, S. Heinze, G. Bihlmayer, A. Kubetzka, O. Pietzsch, S. Blügel, and R. Wiesendanger, Nature (London) **447**, 190 (2007).
[36] C. L. Gao, W. Wulfhekel, and J. Kirschner, Phys. Rev. Lett. **101**, 267205 (2008).
[37] M. Bode, Rep. Prog. Phys. **66,** 523–582 (2003).
[38] A. Kubetzka, M. Bode, O. Pietzsch, and R. Wiesendanger, Phys. Rev. Lett. **88**, 057201 (2002).

[39] C. J. Chen, *Introduction to Scanning Tunneling Microscopy.* New York, Oxford (1993).
[40] J. Tersoff and D. R. Hamann, Phys. Rev. B **31,** 805 (1985).
[41] M. Bode, M. Getzlaff, and R. Wiesendanger, Phys. Rev. Lett. **81**, 4256 (1998).
[42] O. Pietzsch, A. Kubetzka, M. Bode, and R. Wiesendanger, Science **292**, 2053 (2001).
[43] A. Kubetzka, P. Ferriani, M. Bode, S. Heinze, G. Bihlmayer, K. von Bergmann, O. Pietzsch, S. Blügel, and R. Wiesendanger, Phys. Rev. Lett. **94**, 087204 (2005)
[44] S. Meckler, N. Mikuszeit, A. Preßler, E. Y. Vedmedenko, O. Pietzsch, and R. Wiesendanger, Phys. Rev. Lett. **103,** 157201 (2009).
[45] W. Wulfhekel, and J. Kirschner, Appl. Phys. Lett. **75,** 1944 (1999).
[46] H. F. Ding, W. Wulfhekel, and J. Kirschner, Europhys. Lett. **57,** 100 (2002).
[47] U. Schlickum, W. Wulfhekel, and J. Kirschner, Appl. Phys. Lett. **83,** 2016 (2003).
[48] M. Johnson, and J. Clarke, J. Appl. Phys. **67**, 6141 (1990).
[49] C. L. Gao, U. Schlickum, W. Wulfhekel, and J. Kirschner, Phys. Rev. Lett. **98,** 107203 (2007).
[50] C. L. Gao, A. Ernst, A. Winkelmann, J. Henk, W. Wulfhekel, P. Bruno, and J. Kirschner, Phys. Rev. Lett. **100,** 237203 (2008).
[51] H. F. Ding, W.Wulfhekel, J. Henk, P. Bruno, and J. Kirschner, Phys. Rev. Lett. **90,** 116603 (2003).
[52] C. B Wu, P. J. Hsu, H. Y. Yen, and Minn-Tsong Lin, Appl. Phys. Lett. **91,** 202507 (2007).
[53] S. Andrieu, M. Finazzi, P. Bauer, H. Fischer, P. Lefevre, A. Traverse, K. Hricovini, G. Krill, and M. Piecuch, Phys. Rev. B **57**, 1985 (1998).
[54] D. Tulchinsky, J. Unguris, and R. Celotta, J. Magn. Magn. Mater. **212**, 91 (2000).
[55] T. K. Yamada, M.M. J. Bischoff, G.M.M. Heijnen, T. Mizoguchi, and H. van Kempen, Phys. Rev. Lett. **90**, 056803 (2003).
[56] M.-T. Lin, W. C. Lin, C. C. Kuo, and C. L. Chiu, Phys. Rev. B **62**, 14268 (2000).
[57] M. Bischoff, T. Yamada, A. Quinn, and H. van Kempen, Surf. Sci. **501**, 155 (2002).
[58] C. L. Gao, U. Schlickum, W. Wulfhekel, and J. Kirschner, Phys. Rev. Lett. **98**, 107203 (2007).
[59] P. J. Hsu, C. I. Lu, S. W. Chen, W. J. Hsueh, Y. H. Chu, C. H. Hsu, C. J. Butler, and Minn-Tsong Lin, Appl. Phys. Lett. **96,** 142515 (2010).
[60] R. Wiesendanger, Rev. Mod. Phys. **81**, 1495 (2009).
[61] R. Z. Huang, V. S. Stepanyuk, A. L. Klavsyuk, W. Hergert, P. Bruno, and J. Kirschner, Phys. Rev. B 73, 153404 (2006).
[62] K. Tao, V. S. Stepanyuk, P. Bruno, D. I. Bazhanov, V. V. Maslyuk, M. Brandbyge, and I. Mertig, Phys. Rev. B **78**, 014426 (2008).
[63] K. Tao, V. S. Stepanyuk, W. Hergert, I. Rungger, S. Sanvito, and P. Bruno, Phys. Rev. Lett. **103**, 057202 (2009).
[64] O. Pietzsch, A. Kubetzka, M. Bode, and R. Wiesendanger, Phys. Rev. Lett. **92**, 057202 (2004).
[65] O. Pietzsch, S. Okatov, A. Kubetzka, M. Bode, S. Heinze, A. Lichtenstein, and R. Wiesendanger, Phys. Rev. Lett. **96**, 237203 (2006).
[66] N. N. Negulyaev, V. S. Stepanyuk, P. Bruno, L. Diekhoner, P. Wahl, and K. Kern, Phys. Rev. B **77**, 125437 (2008).
[67] L. Diekhöner, M. A. Schneider, A. N. Baranov, V. S. Stepanyuk, P. Bruno, and K. Kern, Phys. Rev. Lett. **90**, 236801 (2003).
[68] M. V. Rastei, B. Heinrich, L. Limot, P. A. Ignatiev, V. S. Stepanyuk, P. Bruno, and J. P. Bucher, Phys. Rev. Lett. **99**, 246102 (2007).
[69] A. Rabe, N. Memmel, A. Steltempohl, and Th. Fauster, Phys. Rev. Lett. **73**, 2728 (1994).
[70] S. Krause, L. Berbil-Bautista, G. Herzog, M. Bode, and R. Wiesendanger, Science **317**, 1537 (2007).
[71] N. Néel, J. Kröger, and R. Berndt, Phys. Rev. Lett. **102**, 086805 (2009).
[72] V. Rodrigues, J. Bettini, P. C. Silva, and D. Ugarte, Phys. Rev. Lett. **91**, 096801 (2003).
[73] M. Bode, O. Pietzsch, A. Kubetzka, S. Heinze, and R. Wiesendanger, Phys. Rev. Lett. **86**, 2142 (2001).
[74] M. Ziegler, N. Ruppelt, N. Néel, J. Kröger, and R. Berndt, Appl. Phys. Lett. **96**, 132505 (2010).

